Available online at www.sciencedirect.com

SciVerse ScienceDirect

Physics Procedia 37 (2012) 309 – 316

Physics Procedia

TIPP 2011 - Technology and Instrumentation for Particle Physics 2011

Total Absorption Dual Readout Calorimetry R&D

B. Bilki[1a,*], Y. Onel[a], A. Para[b], G. Pauletta[c], P. Rubinov[b], I. Vasilas[d], H. Wenzel[b]

[a] *University of Iowa, Iowa City, IA, USA*
[b] *Fermi National Accelerator Laboratory, Batavia, IL, USA*
[c] *INFN Sezione di Trieste, Trieste, Italy*
[d] *University of Cyprus, Nicosia, Cyprus*

Abstract

This calorimetry R&D focuses on establishing a proof of concept for totally active hadron calorimetry. The research program involves evaluating the performance of the different crystal and glass samples in combination with different light collection and readout alternatives to optimize simultaneous collection of Čerenkov and scintillation light components for application of the Dual Readout technique to total absorption calorimetry. We performed initial studies in two short test beam phases in April and November 2010 at Fermilab. Here we present first measurements from these two beam tests.

Keywords:
Dual readout calorimetry, Crystal calorimetry, Total absorption calorimetry, SiPM detectors, Čerenkov detectors, Scintillation detectors

1. Introduction

Measuring the Čerenkov and scintillation light emitted by a hadronic shower developing in transparent absorbing media, the electromagnetic fraction of the shower can be determined, and strong fluctuations of this fraction in the overall energy resolution can be suppressed. This principle is valid also for homogeneous calorimeters (for instance crystals containing heavy elements) and may drastically improve the resolution for hadrons and jets. New photodetectors with high quantum efficiency, photon counting capability and no sensitivity to magnetic fields have promising perspectives towards the applicability of such methods. In particular this last requirement rules out the classic vacuum photomultiplier tubes (PMTs). A new generation of photodetectors with suitable properties may represent a special asset for compensating calorimetry, making it simple, reliable and cheap. An interesting alternative to PMTs has been recently developed and a number of different types of solid state photon counting devices (SiPMs) from various manufacturers are presently becoming commercially available. The potential of these photodetectors has become soon clear but work still needs to be done towards a detailed specification and evaluation in view of different applications and in particular the application of these photosensors to calorimetry.

[1] Also with Argonne National Laboratory, Argonne, IL, USA
[*] E-mail: burak-bilki@uiowa.edu

1875-3892 doi:10.1016/j.phpro.2012.02.382

The purpose of the complete programme of studies is to evaluate the performance of the different crystal and glass samples in combination with different light collection and readout alternatives to optimize simultaneous collection of Čerenkov and scintillation light components for application of the Dual Readout technique to total absorption calorimetry. Crystals are equipped with various optical filters to study the separation of Čerenkov and scintillation light capability via the wavelength separation. Several photodetectors are placed in different positions on the crystal sides to investigate the angular and position dependence of the collected light.

In addition to single crystal studies, R&D also concentrates on the exposure of several electromagnetic crystal calorimeters to investigate the issues associated with larger systems, to establish and check the calibration procedures and to evaluate various potential crystal samples. Electromagnetic calorimeters are expected to provide spatial information and two-photon separation information in addition to the energy measurement.

The R&D also aims to obtain a baseline for the detailed simulations of Čerenkov and scintillation light production in different crystals.

We performed initial studies in two short test beam phases in April and November 2010 at Fermilab Test Beam Facility (FTBF) [1]. Here we present first measurements from these two beam tests where the single crystal with multiple readout as well as different types of crystals were tested.

2. Experimental Setup And Data Acquisition

A 5 x 5 x 5 cm^3 BGO crystal was used to obtain information about Čerenkov and scintillation light yield as a function of time, wavelength, position and photodetector type. All sides of the crystal were equipped with UV or visible filters. Two sides were viewed with PMTs, one through UV and one through visible filter. The remaining four sides were equipped with 9 Hamamatsu SiPMs each [2]. The SiPMs were 1 mm Hamamatsu MPPCs (Multi-Pixel Photon Counters) with 25, 50 and 100 micron pixels, and were placed in a 3 x 3 array on the sides. Figure 1 shows the BGO crystal and the photodetectors.

In order to test the performance of different crytals, arrays of 6 BGO and 6 PbF_2 samples were used. All crystals were 5 cm in length but were different in cross sections (2 x 2, 3 x 3 and 4 x 4 cm^2). All were read out by 3 mm Hamamatsu MPPCs located at the center of the downstream face. The crystals had different wrapping (black paper or Tyvek) and different surface finishes to provide information about light collection for Čerenkov (PbF_2) and scintillation (BGO) as a function of crystal geometry and surface condition.

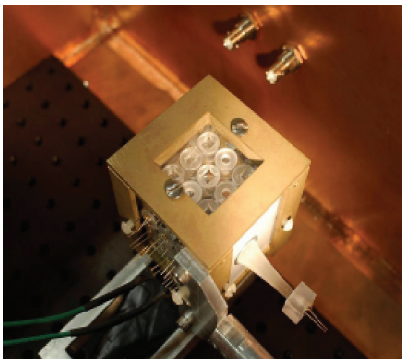

Fig. 1. BGO crystal with several photodetectors on the sides with UV and visible filters.

The photodetectors were read out using the latest generation of the Fermilab TB4 boards designed explicitly for calorimetry applications. Four mother boards with four daughter cards each provide 64 channels of waveform digitizers with a sampling rate of 220 MHz.

For the tests mentioned in this paper, 120 GeV/c primary proton beam of the FTBF was used. Figure 2 shows the test setup on the motion table. The red arrow indicates the beam direction. TB4 boards and the dark boxes for the BGO and PbF_2 crystal arrays can be seen downstream and to the right of the single BGO crystal box respectively. The events were triggered by the coincidence of two scintillation counters.

Fig. 2. Test setup on the motion table. The red arrow indicates the beam direction.

3. SiPM Calibration

We used 11 settings as the bias voltages of the SiPMs denoted by "step" -5 to 5 in increments of 1 throughout this text with "step 5" being the lowest bias voltage. The pedestal mean and rms values obtained per time sample in a 400 time sample window are shown in Fig. 3. Channels 0 and 1 are the PMTs viewing the single BGO crystal through visible and UV filters respectively, and channels 2 and 3 are the trigger PMTs. Hence they show no variation under bias voltage changes. Channels 4 through 39 are the SiPMs of the single BGO crystal, and the channels 40 through 51 are the SiPMs of the BGO and PbF_2 crystal arrays.

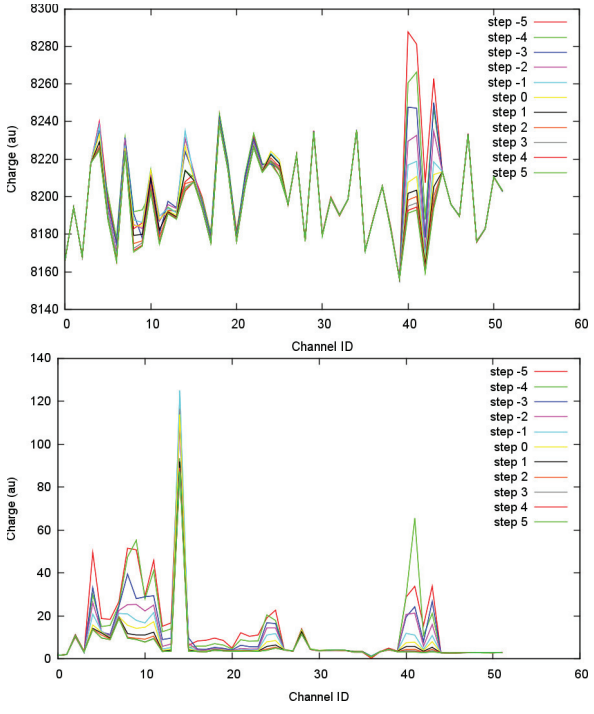

Fig. 3. Pedestal mean (top) and rms (bottom) values per time sample for all channels.

Figure 4 shows a sample waveform after pedestal subtraction and zero suppression. The optimal bias voltage setting was selected to provide minimal afterpulses and clean single avalanche peaks as can be seen in Fig. 4.

At this stage, various methods of calibration can be chosen. In this preliminary analysis, we studied two approaches: The single avalanche peaks are identified by either looking at the spectrum of all the amplitudes or the maximum amplitudes in the waveforms. Then the pulses with the right amplitudes are integrated to obtain the single avalanche charges. Figure 5 examplifies both methods. Figure 5a shows the spectrum for all amplitudes in the waveform where a lower threshold of 10 can be set to search for single avalanche peaks, and Fig. 5b shows the spectrum for the maximum amplitudes and that a search for single avalanche pulses can be performed within the range 20 - 40 units of amplitude. The resulting single avalanche charge integrals are shown in Fig. 5c and Fig. 5d respectively. The fits to the single avalanche charge peaks with gaussians yield similar values for both methods. It is notable that the multiple avalanche peaks are also observable.

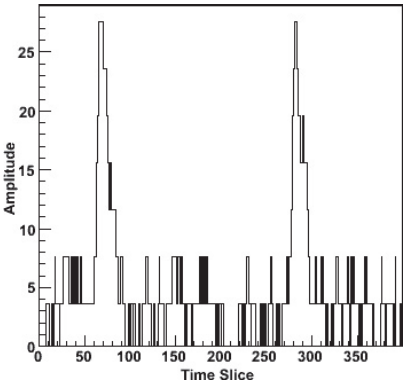

Fig. 4. Sample waveform after pedestal subtraction and zero suppression. Each time slice correcponds to ∼ 4.5 ns. Pedestal fluctuations are visible in the entire readout window.

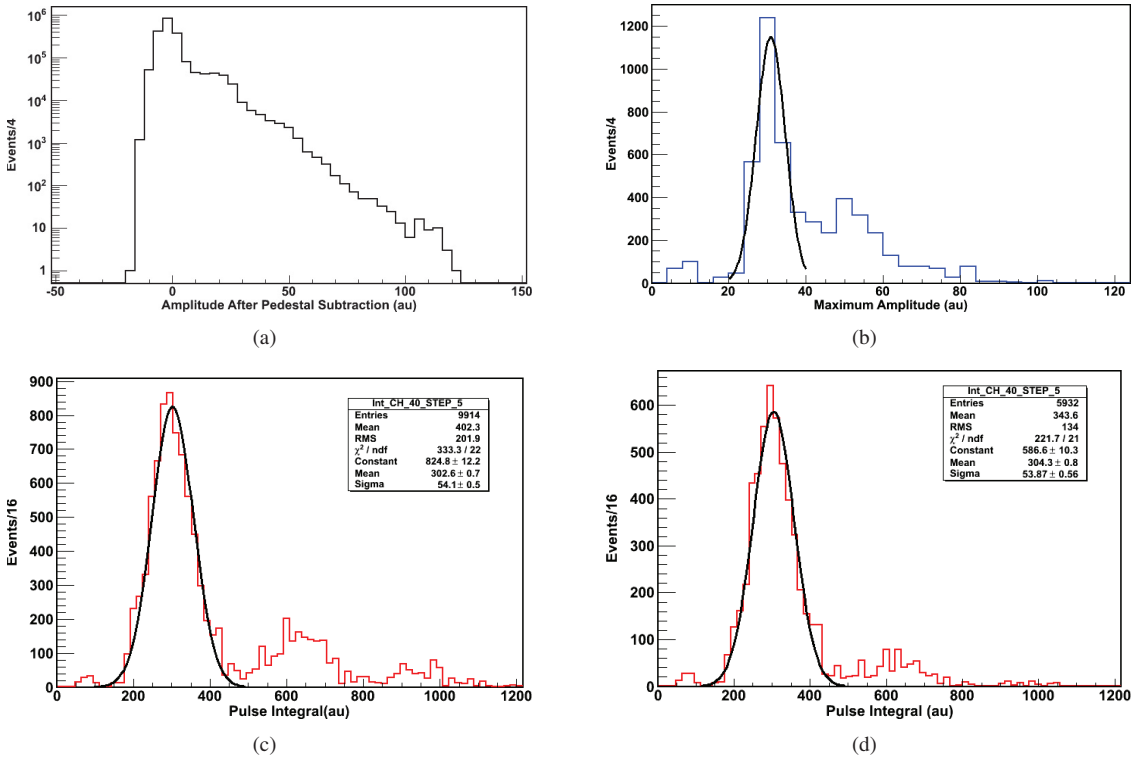

Fig. 5. The spectra for all amplitudes (a) and maximum amplitudes (b) in the pedestal subtracted and zero suppressed waveforms, and the corresponding spectra for pulse integrals (c and d) together with the fits to the single avalanche peaks.

4. Tests With The BGO and PbF_2 Crystal Arrays

Figure 6 shows a sketch of the BGO and PbF_2 crystal arrays as seen by the beam. The beam was centered on each crystal and the signal was readout by 3 mm Hamamatsu MPPCs placed at the center of the downstream face.

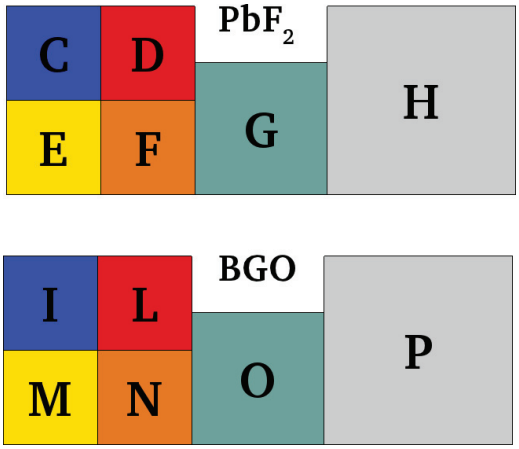

Fig. 6. A sketch of the crystal arrays box as seen by the beam (not to scale).

Figure 7 shows the average waveforms for O (a), P (b) and M (c) crystals. The integrals of these average pulses provide information about the relative magnitude of the scintillation signals generated in these BGO crystals. The integrals are around 750, 600 and 400 avalanches for the O, P and M crystals respectively. Lateral sizes of the O, P and M crystals are 3 x 3 cm^2, 4 x 4 cm^2 and 2 x 2 cm^2. The wrapping materials and the crystal geometries quantitatively effect the overall signal.

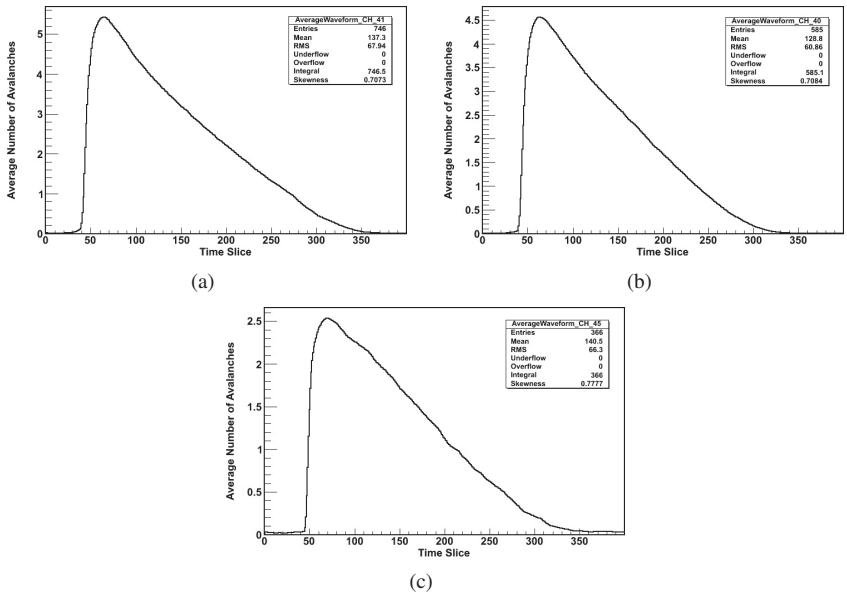

Fig. 7. Average waveform per event in units of avalanches for O (a), P (b) and M (c) BGO crystals.

Figure 8 shows the average waveforms for G (a), C (b) and H (c) crystals. The integrals are around 80 avalanches for the G and H crystals, and around 20 avalanches for the C crystal and provide information about the Čerenkov light production in PbF_2 crystals.

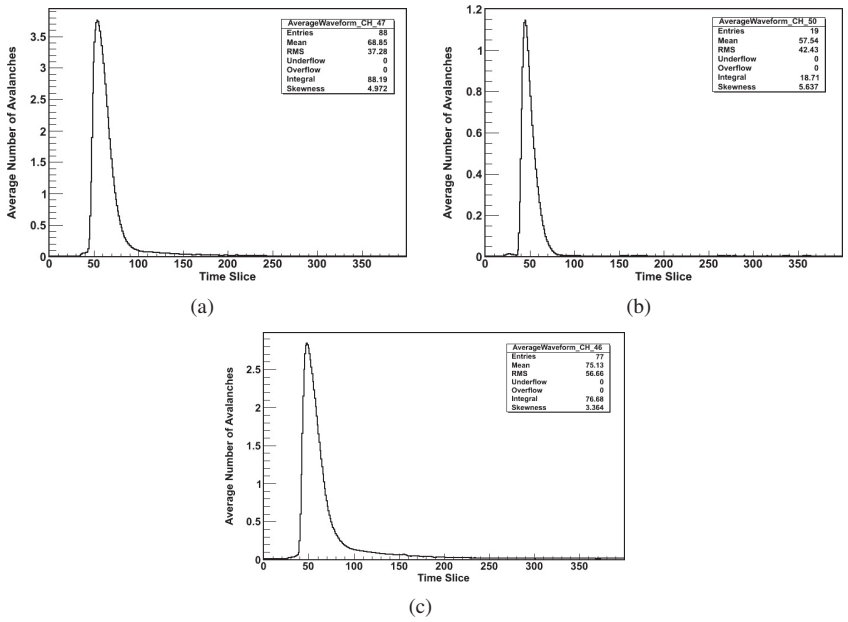

Fig. 8. Average waveform per event in units of avalanches for G (a), C (b) and H (c) PbF_2 crystals.

The magnitude of the scintillation signals in BGO crystals is about an order of magnitude larger than that of the Čerenkov signals in PbF_2 crystals and the scintillation pulses are a factor of 6 wider than the Čerenkov pulses. These provide a valuable input to a better understanding of the Čerenkov and scintillation light production mechanisms and to detailed simulations of various conditions and applications. For both light production mechanisms, the signal detection is observed to be dependent on the surface finishes, wrapping conditions and the lateral size of the crystals. An enhanced simulation framework is aimed to describe both mechanisms for different crystal types under different physical conditions and with different readout systems.

Overall, these tests show that arrays of crystals with directly coupled SiPM readouts can have immediate calorimetric implementations upon a careful study of the crystal properties including Čerenkov and scintillation light yields, effects of geometric factors, crystal and photodetector couplings and transverse segmentation.

5. Tests With The Single BGO Crystal

Figure 9 shows a sketch of the single BGO crystal with many photodetectors. The right and left sides are read out by PMTs through visible and UV filters, the upstream and downstream faces are read out by SiPMs through visible and UV filters respectively, and the top and bottom faces are read out by SiPMs through visible and UV filters respectively.

The emission spectrum of the BGO peaks at around 480 nm and covers almost all of the visible spectrum. Most Čerenkov radiation is in the ultroviolet region of the spectrum and is a continously falling function of the wavelength. Therefore, the visible filters are selected to filter out the scintillation light whereas the UV filters are for measuring the Čerenkov light.

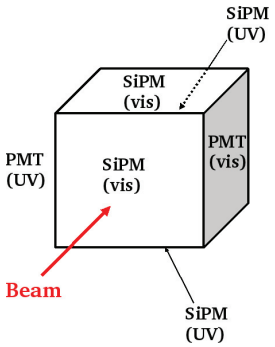

Fig. 9. A sketch of the single BGO crystal.

Figure 10 shows sample waveforms of single events for a top (Fig.10a), front (Fig.10b), back (Fig.10c) and bottom (Fig.10d) SiPM. The top and front SiPMs read around 200 and 330 avalanches as scintillation signals, and the back and bottom SiPMs read around 6 and 3 avalanches as Čerenkov signals respectively. The characteristics of the Čerenkov and scintillation signals are evident from the pulse shapes. The scintillation signals are wider and have larger magnitudes when compared to the Čerenkov signals. The isotropic nature of scintillation is realized with the comparable amplitudes of the signals from the top and front SiPMs, and the directional nature of the Čerenkov process is realized with the difference between the signals from the back and bottom SiPMs. In both cases, the signals can be read out by SiPMs that are directly coupled to the crystal. The optical filters successfully discriminate the Čerenkov and scintillation components.

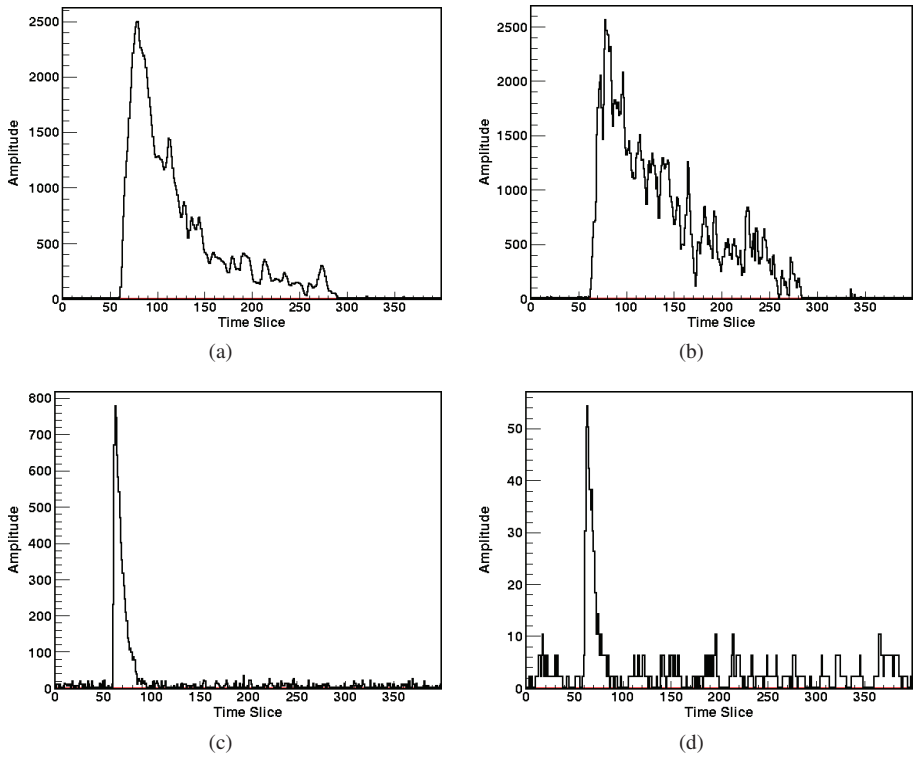

Fig. 10. Sample waveforms for a top (a), front (b), back (c) and bottom (d) SiPM.

6. Summary

We tested a single BGO crystal equipped with many SiPMs and PMTs on all sides that read out through different optical filters in order to investigate the spatial and time development of Čerenkov and scintillation signals, and arrays of BGO and PbF_2 crystals with different surface finishes, wrappings and geometries in order to study the effects of these variables on the Čerenkov and scintillation light production.

The preliminary analysis presented here indicates that both Čerenkov and scintillation signals are observed with SiPMs coupled directly to the crystals. The two mechanisms are observed to produce distinctive waveforms both in terms of amplitudes and timing. The optical filters provide measurable separation of the two light components. The geometrical factors as well as crystal surface and coupling conditions are effective on the production and detection of the Čerenkov and scintillation signals. These effects also vary by different crystal types.

The detailed simulations of Čerenkov and scintillation light production mechanisms and readout methods, which is within the complete analysis programme, would enable the demonstration of the proof of concept for totally active hadron calorimetry and the enhanced modeling of total absorption dual readout calorimeters for future colliders.

References

[1] Fermilab Test Beam Facility, http://www-ppd.fnal.gov/FTBF/.
[2] Hamamatsu Web Site, http://www.hamamatsu.com/.